

## Gamma Ray Source Studies Using Muon Tracking

---

**Paul Doll for KASCADE-Grande<sup>\*†</sup>**

*KIT Karlsruhe Campus North, Germany*

*E-mail: paul.doll@kit.edu*

A large area ( $128 \text{ m}^2$ ) streamer tube detector, located within the KASCADE-Grande experiment, has been built with the aim to identify by track measurements muons from extensive air showers and to reconstruct their directions. We discuss the possibility of observing gamma ray sources by means of photo-pion produced single isolated muons, on top of the background of muons generated by charged cosmic-rays, using a well shielded muon tracking detector (MTD) of good pointing accuracy. Properties of the photo-production process and of the MTD which support the identification of gammas are discussed.

*36th International Conference on High Energy Physics,  
July 4-11, 2012  
Melbourne, Australia*

---

<sup>\*</sup>Speaker.

<sup>†</sup><http://www-ik.fzk.de/KASCADE-home.html>

## 1. Introduction

Muon tracking detectors (MTD) [1] did successfully demonstrate that detectors, which measure the angle of each track, can be used to improve the precision in the measurement of the primary particle direction, because the directions of muons are much better correlated with the primary CR direction than any other secondary particle component in an extensive air shower (EAS) [2, 3, 4]. High energy gamma rays produce muons in the Earth's atmosphere that can be detected and reconstructed in relatively shallow underground muon detectors. Although muons of such low energy are mostly produced by charged CRs, gamma produced muons can be identified, provided the detector has sufficient effective area and resolution. Unlike air-Cherenkov telescopes muon detectors cover a large fraction of the sky with a large duty cycle. The advantage is considerable in studying the emission from highly variable sources. Moreover, background multi-muon bundles can be conveniently rejected without suppression of the predominantly single-muon gamma signal. Muons of  $E_\mu \geq 1 \text{ GeV}$  associated with primary photons of several tens of GeV provide an almost attenuation-free window into the full depth of the Universe, suffering little from flux losses due to collisions with IR and CMB radiation via electron pair production.

## 2. Gamma versus Proton induced Showers

The Vector Meson Dominance Model is usually employed for photo-nuclear interactions at gamma energies above a few GeV. The critical role played by the event generators in predicting the muon content of showers, is shown by the FLUKA code in Ref. [5] for both gammas and protons at 100 GeV. Fig. 1 in Ref. [5] emphasizes a basic difference between gamma and proton induced showers. Gamma primaries lead to a large fraction of high-x secondaries. Proton primaries produce dominantly low-x pions. Proton induced multiple interactions in the atmosphere lead to relatively large angles, while a Gamma induced photo-pion process is confined to very forward direction according to FLUKA simulations [6]. Valuable studies for gamma induced EAS show that most muons are produced from tens of GeV photons [7, 8, 9].

Valuable simulation work from ref. [6] did provide e.g. Fig. 1 where the dashed curve represents a gamma flux spectrum impinging on the Earth atmosphere with a slope for the differential flux of  $\alpha = 2.41$ . At low energy the gamma flux is strongly absorbed in the atmosphere ( $\lambda_{em}^{air} \approx 60 \text{ gcm}^{-2}$ ) what has an immediate impact on the number of muons reaching sea level per primary photon  $N_\mu/N_\gamma$ . The resulting muon flux spectrum as a function of primary gamma energy  $d\Phi_\mu/dE_\gamma$  points to an integral dependence of the muon yield on  $E_\gamma$  and, therefore, to an effective gamma flux increase at threshold. The number of muons with energy above a threshold energy  $E_\mu$  in a shower initiated by a photon of energy  $E_\gamma$  is given by Halzen et al. [13] in an analytical form, where energies are adequate for  $E_\gamma/E_\mu > 10$ . The number of gamma events in a detector of effective area  $A_{MTD} = 128 \text{ m}^2$  [2] for  $E_\gamma$  above 10 GeV amounts to  $S_\mu \approx 50$  muons per day to be detected from Crab in the MTD. However the Mkn 421 source provided during its high flux flaring episode (February-March 2010) an about 10 times higher flux than Crab [10, 14, 15, 16], making analysis a lot easier. Fig. 1 indicates that a muon energy cut equal to 0.15 GeV is sensitive to the gamma energy region above about 10 GeV. Experimental studies (see Fig. 2) allow to determine the background muons from charged CRs. Above a muon energy of 0.8 GeV in a  $0.25^\circ \times 0.25^\circ$  pixel

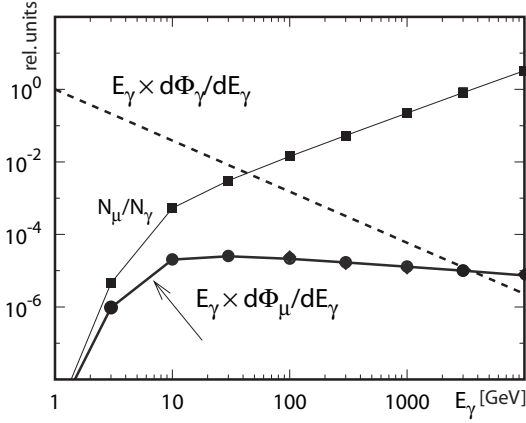


**Figure 1:** Simulation results (from ref. [6]) of the following quantities as a function of gamma ray energy: the energy spectrum of the primary gamma rays ( $d\Phi_\gamma/dE_\gamma$  - dashed line), the multiplicity of muons at sea level ( $E_\mu > 0.15 \text{ GeV}$ ) per primary gamma ray ( $N_\mu/N_\gamma$  - filled squares) and the result of folding those two ( $d\Phi_\mu/dE_\gamma = N_\mu/N_\gamma \times d\Phi_\gamma/dE_\gamma$  - filled circles). The calculated values are joined with lines to guide the eyes. Note that the differential fluxes are multiplied by  $E_\gamma$ .

$N_\mu \approx 40$  background muon tracks per day are obtained. This pixel size is supported by the strong focusing of the gamma induced muons. This rate leads for Crab to an estimated  $S_\mu/N_\mu^{1/2} \approx 10$  for 50 h of free data taking.

### 3. Gamma Sources

To identify sources which emit high energy gammas and which are converted to single isolated muons, we have the possibility to restrict the arrival direction and arrival time. In the analysis [4] we use bin size  $\Delta\delta = 0.25^\circ$  and  $\Delta\alpha = 0.8\Delta\delta/\cos\delta$  confined to specific regions on the sky to investigate the MTD [2] sensitivity to specific gamma ray sources. Only specific arrival time periods, where the corresponding source is high above the observer are chosen to accumulate clean single muon events in the  $\delta \times \alpha$  plane. Gamma primaries above 10  $\text{GeV}$  produce on average equal numbers of  $\mu^+$  or  $\mu^-$  from  $\pi^+$  or  $\pi^-$  decays. When we restrict the MTD track analysis to single isolated tracks with no accompanying particles we reduce the background muons from CRs by about 2 orders of magnitude in a  $0.25^\circ \times 0.25^\circ$  bin in the sky. The selection of gamma-like tracks leads to West deflection for  $\mu^-$  and East deflection for  $\mu^+$  [6, 11] at the geographical location ( $49^\circ$  North) of the MTD.

Mkn 421 was studied in the zenith angle range  $\Theta = 2^\circ - 22^\circ$ . The source is a very active Galaxy Nucleus showing strong variation in the X-ray and TeV gamma ray fluxes [17, 18] and a hard ( $\alpha = 1.90$ ) differential flux spectrum [14]. From our muon tracking analysis the source is shown in Fig. 2 at 11.08 h,  $37.9^\circ$ , which is  $\approx 0.1^\circ$  further away from the zenith and  $\approx 0.1^\circ$  later in time, with respect to the known position. This position is achieved [4] from negatively charged muons employing a correction for the deflection of the muons proportional to the geomagnetic field  $B_{geo}$ :  $B_E = 0.0, B_N = 0.2, B_V = 0.5$  in units of Gauss for the East, North and vertical component, respectively [12]. This correction focuses on the dominating muon flux at the momentum threshold

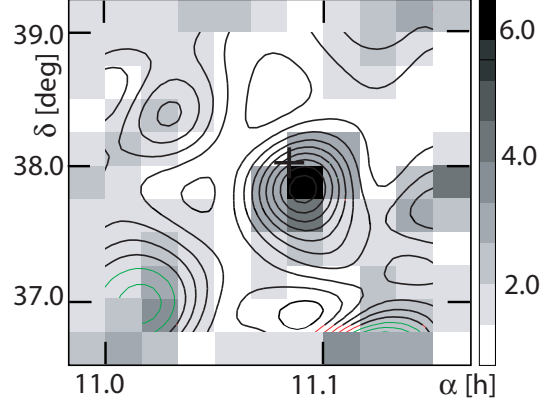


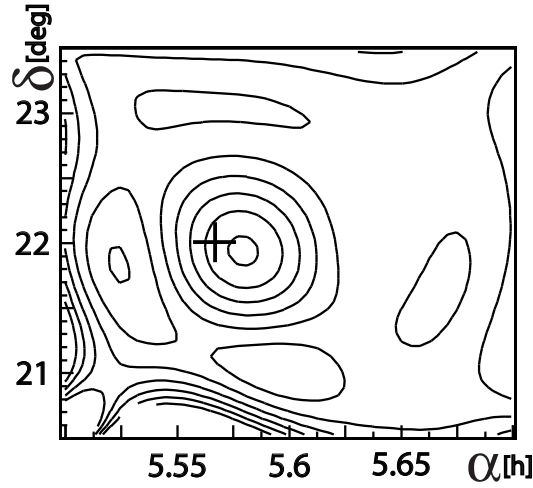
**Figure 2:** Single muon flux close to Mkn 421 source position (cross [19]), color code is in units of standard deviation and contour lines are a maximum-likelihood fit [20] to the bin contents. Data were taken during a X-ray [16] high flux flaring episode during February-March 2010.

(0.8 GeV) (higher significance) and assumes a constant muon production height. The position of the high energy gamma source studied with the MAGIC telescope [19] is given by the cross in Fig. 2. Interestingly, the source significance in Fig. 2 is improved when employing days for which appreciable X-ray flux ( $> 2.5$ ) counts / sec is reported [10].

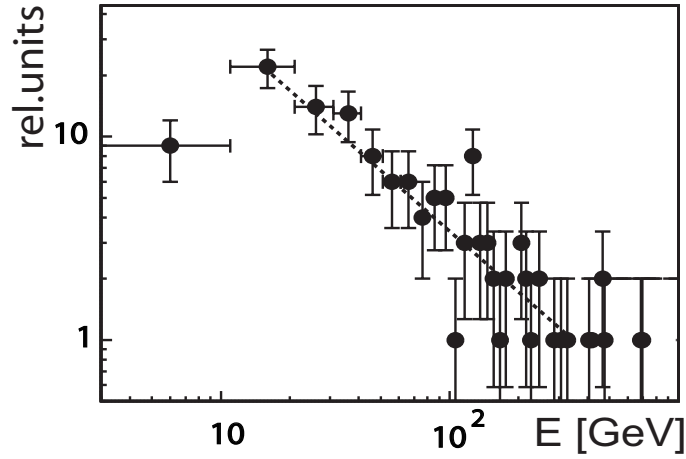
Crab was studied in the fairly inclined zenith angle range  $\Theta = 20^\circ - 40^\circ$  and appears in single muon tracking (Fig. 3) at 5.56 h,  $21.9^\circ$  which is  $\approx 0.1^\circ$  further away from the zenith and  $\approx 0.1^\circ$  later in time, compared to the known position of the Crab source. This position is achieved employing moderate corrections for the deflection of the muons proportional to the geomagnetic field  $B_{geo}$  [12] effecting dominantly muons at the momentum threshold (0.8 GeV). The position of the source as quoted by the MAGIC group [19] is given by the cross in Fig. 3.

Fig. 3 shows a contour plot describing a maximum-likelihood fit [20] to the bin contents sampled over a grid of bin size  $\Delta\delta = 0.25^\circ$  and  $\Delta\alpha = 0.9\Delta\delta/\cos\delta$  and smoothed afterwards, employing high quality muon tracks weighted according to actual MTD efficiency. The contour scale is in units of excess counts per smoothing radius [20]. The displacement of the source position and possible deformation is due to the geomagnetic field  $B_{geo}$  and is expected to depend on the momentum and production height of the muons and their orientation with respect to the geomagnetic field components [12].

Gamma induced single isolated muon tracks (without correction for  $B_{geo}$ ) for negatively charged muons can be identified as being bend ( $\delta_\mu$ ) towards the West from the actual Crab source position. Only negatively charged muons which bend to the West side of the source position are considered to fill an angular distance spectrum. The frequency of muon tracks as function of  $(1/\delta_\mu)$  is plotted in Fig. 4, resulting in steeply falling spectrum. The inverse angular distance is transformed to muon momentum assuming a constant mean muon production height, a  $p_\mu \times B_{geo}$  dependence and a muon momentum threshold of 0.8 GeV. In Fig. 4 the relative differential negative muon flux versus muon momentum is shown. FERMI-LAT observations [21] report for the differential gamma



**Figure 3:** Single muon flux close to Crab source position [19]. Contour lines are a maximum-likelihood fit [20] to the bin contents. Data were taken when  $\Theta_{Crab} \leq 35^\circ$ .



**Figure 4:** Relative negative muon flux close to Crab position as function of muon momentum assuming  $E = 10 \times p_\mu$ . Dashed line shows a fit with spectral slope  $\approx 1.0$ .

flux two different slopes in this gamma energy range for the Crab nebula ( $\alpha = 1.89$ ) and Crab pulsar ( $\alpha = 2.08$ ), respectively. According to the spectral slopes observed in Fig. 1 an improved  $E_\mu/E_\gamma$  relation may lead to a  $E_\gamma^{-(\approx 0.8)}$  dependence. The scatter of the data points at high muon momentum are due to the finite angular resolution and/or background contributions. For gamma sources with an even harder energy spectrum a muon momentum spectrum can possibly be derived when recording data during larger inclination with respect to the geomagnetic field.

#### 4. Conclusions

High resolution muon tracking may provide a ground based technique for a wide field of view and large duty cycle observations of gamma sources at a gamma energy threshold of tens of GeV. The behavior and influence of the atmospheric conditions has to be further studied. The recording

of temperature and pressure has to be improved by monitoring the isobars for different weather conditions.

## 5. Acknowledgements

This work was supported by the KIT Campus Nord Karlsruhe, the BMBF of Germany, the MIUR and INAF of Italy, the Polish Ministry of Science and Higher Education, the Romanian Authority for Scientific Research UEFISCDI (PNII-IDEI grants 271/2011 and 17/2011).

## References

- [1] J. Gress *et al.*, Nucl. Instr. and Meth. **A302** (1991) 368. L. Horton *et al.*, Nucl. Instr. and Meth. **A325** (1993) 326. M. Feuerstack *et al.*, Nucl. Instr. and Meth. **A315** (1992) 357.
- [2] P. Doll *et al.*, KASCADE Coll., Nucl. Instr. and Meth. **A488** (2002) 517.
- [3] W.D. Apel *et al.*, KASCADE-Grande Coll., Astropart.Phys. **34** (2011) 476.
- [4] P. Doll *et al.*, KASCADE-GrandeColl., submitted to Nucl. Instr. and Meth.
- [5] A. Fasso and J. Poirier, Phys.Rev. **D63** (2001) 036002.
- [6] J. Poirier, S. Roesler and A. Fasso, Astropart.Phys. **17** (2002) 441.
- [7] P. Achard *et al.*, L3 Coll., Astropart.Phys. **25** (2006) 298.
- [8] T.K. Gaisser, F. Halzen and T. Stanev, Phys.Reports, **258** (1995) 173.
- [9] P. LeCoultré *et al.*, L3 Coll., Nucl.Phys. B(Proc.Suppl.) **122** (2003) 161.
- [10] <http://www.swift.psu.edu/monitoring>
- [11] D. Heck *et al.*, Report FZKA 6019, Forschungszentrum Karlsruhe (1998).
- [12] Int. Association of Geomagnetism and Aeronomy (IAGA) <http://www.ngdc.noaa.gov/IAGA>
- [13] F. Halzen, T. Stanev and G.B. Yodh, Phys.Rev. **D55** (1997) 4475.
- [14] N. Galante *et al.*, VERITAS Coll., Proc. 32th ICRC (2011) Beijing, China, 0782.  
<http://galprop.stanford.edu/elibrary/icrc2011/index.html>
- [15] <http://fermi.gsfc.nasa.gov/ssc/data>
- [16] <http://xte.mit.edu/asmlc>
- [17] S. Vernetto *et al.*, ARGO-YBJ Coll., Proc. 31th ICRC (2009), Lodz, Poland  
<http://icrc2009.uni.lodz.pl/proc/pdf/icrc0398.pdf>
- [18] M. Blazejowski *et al.*, WHIPPLE Coll., The ApJ **630** (2005) 130.
- [19] E. Aliu *et al.*, MAGIC Coll., Science **322** (2008) 1221.
- [20] J. Allison, Comp. Phys. Communication **77** (1993) 377.
- [21] M.H. Grondin *et al.*, FERMI-LAT Coll., Proc. 31th ICRC,(2009), Lodz, Poland  
<http://icrc2009.uni.lodz.pl/proc/pdf/icrc1141.pdf>